AD-A268 366

ATION PAGE

Form Approved
OMB No. 0704-0188

response, including the time for reviewing instructions, searching existing data sources, gathering and maintaining the data needed, burden estimate or any other aspect of this collection of information, including suggestions for reducing this burden, to Washington Davis Highway, Suite 1204, Arlington, VA 22202-4302, and to the Office of Management and Budget, Paperwork Reduction Project

1. AGENCY USE ONLY (*Leave blank*)	2. REPORT DATE	3. REPORT TYPE AND DATES COVERED
	10 MAY 1993	JOURNAL ARTICLE

4. TITLE AND SUBTITLE
DESIGN AND FABRICATION OF A GAUSSIAN FAN-OUT OPTICAL INTERCONNECT

5. FUNDING NUMBERS
C — F19628-90-C-0002
PE — 62702E

6. AUTHOR(S)
V.V. WONG, G.J.SWANSON

DTIC
ELECTE
AUG 11 1993
S A D

7. PERFORMING ORGANIZATION NAME(S) AND ADDRESS(ES)
Lincoln Laboratory, MIT
P.O. Box 73
Lexington, MA 02173-9108

8. PERFORMING ORGANIZATION REPORT NUMBER
JA-6802

9. SPONSORING/MONITORING AGENCY NAME(S) AND ADDRESS(ES)
DEFENSE ADVANCED RESEARCH PROJECTS AGENCY
3701 N. FAIRFAX DRIVE
ARLINGTON, VA 22203

10. SPONSORING/MONITORING AGENCY REPORT NUMBER
ESC-TR-93-246

11. SUPPLEMENTARY NOTES
APPLIED OPTICS/VOL.32, NO.14/ 10 MAY 1993

12a. DISTRIBUTION/AVAILABILITY STATEMENT
Approved for public release; distribution is unlimited.

12b. DISTRIBUTION CODE

13. ABSTRACT (*Maximum 200 words*)

A phase-retrieval algorithm is described and used to optimize the phase profile of a multilevel phase grating that achieves a two-dimensional Gaussian fan-out. Binary-optics technology is used to fabricate a surface-relief structure that implements this optimized phase profile. The results of the fabrication process are summarized, and the experimental measurements on the fan-out element are presented. Differences between theory and experiment arise from scalar-theory approximations used in the design algorithm. In order to illustrate the scalar-theory limitations, a rigorous formulation is used to analyze the diffraction efficiency and the reconstruction error of a representative binary surface-relief phase grating as a function of the period-to-wavelength ratio. The analysis serves to show qualitatively the effects of the period-to-wavelength ratio on the performance of free-space optical interconnects designed with a scalar-theory formalism.

14. SUBJECT TERMS
Key words: Optical interconnects, binary optics, holographic optical elements, computer-generated holograms.

15. NUMBER OF PAGES
10

16. PRICE CODE

17. SECURITY CLASSIFICATION OF REPORT	18. SECURITY CLASSIFICATION OF THIS PAGE	19. SECURITY CLASSIFICATION OF ABSTRACT	20. LIMITATION OF ABSTRACT
Unclassified	Unclassified	Unclassified	

a reprint from Applied Optics

Design and fabrication of a Gaussian fan-out optical interconnect

Vincent V. Wong and Gary J. Swanson

A phase-retrieval algorithm is described and used to optimize the phase profile of a multilevel phase grating that achieves a two-dimensional Gaussian fan-out. Binary-optics technology is used to fabricate a surface-relief structure that implements this optimized phase profile. The results of the fabrication process are summarized, and the experimental measurements on the fan-out element are presented. Differences between theory and experiment arise from scalar-theory approximations used in the design algorithm. In order to illustrate the scalar-theory limitations, a rigorous formulation is used to analyze the diffraction efficiency and the reconstruction error of a representative binary surface-relief phase grating as a function of the period-to-wavelength ratio. The analysis serves to show qualitatively the effects of the period-to-wavelength ratio on the performance of free-space optical interconnects designed with a scalar-theory formalism.

Key words: Optical interconnects, binary optics, holographic optical elements, computer-generated holograms.

1. Introduction

Free-space optical interconnects are optical elements that split a single laser beam into a one-dimensional (1-D) or two-dimensional (2-D) array of beams.[1,2] These interconnects are essential components in many applications of modern optics, such as optical parallel processing and neural computing,[3,4] in which it is necessary to multiplex light from a single source upon many detectors. There are two characteristics of a free-space optical interconnect: The degree of connectivity, or fan-out, and the splitting ratio. The fan-out is a measure of the number of detectors connected to each source. Clearly, conventional refractive optical elements cannot be used to achieve the fan-out. Rather, diffractive optical elements, particularly phase gratings, which can split an incoming beam into many beams or diffraction orders, must be used. The splitting ratio describes the relative power directed into each of the diffraction orders of the grating. The problem at hand therefore is to design a free-space optical interconnect, given a specification of its degree of fan-out and its splitting ratio. In general, an exact solution for the grating phase profile in this framework does not exist; however, by optimizing the grating phase profile over one period, we can approximate a specified grating angular spectrum.

Several phase-optimization techniques exist. Simulated-annealing[5] and the Gerchberg–Saxton phase-retrieval[6] algorithms are two of the most popular. The former technique is well suited for the optimization of binary phase profiles, while the latter technique is better adapted for the optimization of continuous phase profiles. Here we employ a modified Gerchberg–Saxton phase-retrieval algorithm to optimize a multilevel phase profile that achieves a 1-to-11 Gaussian fan-out in two dimensions (i.e., an 11 × 11 array of light spots). This element will be used for an optical processing system that serves as an artificial retina.[7] Section 2 describes the algorithm and presents the results of the optimization.

Optimized phase profiles are implemented with surface-relief structures by etching away selected regions of a grating substrate. Section 3 describes briefly the binary-optics fabrication process that is used to form such surface-relief structures and presents the fabrication results of the above multilevel surface-relief phase grating. The measured etch depths are considered and compared with the target etch depths determined from the phase-optimization procedure. The experimental measurements of the grating power spectrum are presented in Section 4. These measured values are compared

The authors are with the Lincoln Laboratory, Massachusetts Institute of Technology, 244 Wood Street, Lexington, Massachusetts, 02713-9108.

Received 6 March 1992.
0003-6935/93/142502-10$05.00/0.

with predicted values calculated by using a Fourier-optics formalism of grating diffraction.

Both the simulated-annealing and phase-retrieval algorithms utilize scalar diffraction theory, which is an approximate theory derived from Maxwell's equations. Scalar diffraction theory provides an accurate description of grating diffraction for large period-to-wavelength ratios. Therefore the results and predictions of such a theory (i.e., optimized phase profiles) are consistent with experimentally observed phenomena if the physical period of the grating is large compared with the wavelength of the incident radiation.

To predict the diffraction behavior of gratings with small period-to-wavelength ratios, we must use a rigorous formulation of grating diffraction. Of course, a rigorous analysis can be carried out to describe all grating diffraction phenomena; however, such an analysis is computationally intensive. This fact limits the usefulness of a rigorous theory in the design of free-space optical interconnects. In contrast, scalar diffraction theory results in a simple Fourier-transform relation, which is ideally suited for numerical computation, between the grating transmittance function and the grating angular spectrum. Therefore to maintain the integrity of the solutions obtained from phase-optimization techniques based on scalar diffraction theory, it is important to investigate the conditions under which scalar diffraction theory can be used to accurately describe the diffraction characteristics of actual surface-relief phase gratings.

In Section 5 we apply a rigorous formulation of grating diffraction[8] to analyze the diffraction behavior of a representative binary surface-relief structure as a function of the period-to-wavelength ratio. This structure is a practical implementation of a binary phase profile that, in the large period-to-wavelength regime, achieves a 1-to-5 uniform fan-out. The grating performance, as a function of the period-to-wavelength ratio, is evaluated based on diffraction efficiency and reconstruction error.

2. Phase-Optimization Algorithm

A. Background

In the scalar limit, the grating transmittance function and the grating angular spectrum are related through a Fourier transform. In designing free-space optical interconnects, constraints on both the transmittance function (i.e., phase-only) and the angular spectrum (i.e., a desired power spectrum) are imposed. The technique of phase retrieval,[6] first developed by Gerchberg and Saxton, accounts for these constraints in an iterative Fourier-transform algorithm for the optimization of the grating phase.

The Gerchberg–Saxton phase-retrieval algorithm results in a phase profile that varies continuously and is extremely difficult to fabricate. However, this continuous phase profile can be well approximated by quantizing a modulo-2π version of the continuous phase profile into 2^L phase levels, where L is a positive integer. This modulo-2π quantization operation ($\mathrm{MOD}_{2\pi}/Q_M$), where M denotes the number of phase levels used in the stepwise approximation, is the basis of the binary-optics fabrication process[9] and can be incorporated directly into the Gerchberg–Saxton phase-retrieval algorithm. This modified phase-retrieval algorithm permits optimization of phase profiles that can in practice be fabricated with existing technologies. A block diagram of the modified phase-retrieval algorithm is shown in Fig. 1. A similar quantization scheme has been used to code computer-generated holograms.[10] The incorporation of a quantization operation into the phase-retrieval algorithm can potentially cause the algorithm to stagnate if the number of quantization levels is small. We employed a quantization of 16 phase levels and had no problems with the algorithm stagnating.

The object space corresponds to the grating, and the image space corresponds to the grating angular spectrum. The grating transmittance is represented by amplitude distribution $t(l, p)$ and phase distribution $\Phi(l\ p)$. Similarly, the grating's angular spectrum is described by amplitude and phase distributions $T(n, m)$ and $\Theta(n, m)$, respectively. The basic idea of using the algorithm is to Fourier transform back and forth between these domains, while satisfying the constraints in one domain before returning to the other domain. As shown, the object domain constraint is that the grating transmittance have unit magnitude (i.e., phase only), while the image domain constraint is that the magnitude of the angular spectrum be Gaussian. The Gaussian shape imposed on the magnitude of the angular spectrum is represented by the function

$$G(n, m) = \exp -[\sigma(n^2 + m^2)], \qquad (1)$$

where the parameter σ determines the desired width of the Gaussian fan-out distribution.

The algorithm starts in the object domain with an initial guess of the grating transmittance function, $t_0(l, p)$. Since the grating is to be phase only, the

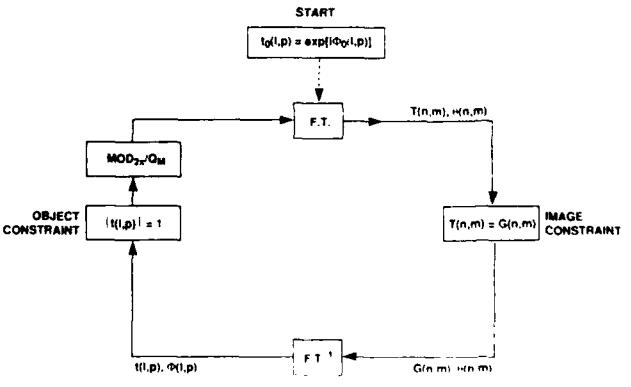

Fig. 1. Block diagram of modified phase-retrieval algorithm.

estimate is typically implemented as a random configuration of phases,[6,11] which we denote $\Phi_0(l, p)$, where l and p are the array indices that span a single period of the phase grating. The initial phase configuration that was used is obtained by

$$\Phi_0(l, p) = 2\pi\beta \exp\left\{-\alpha\left[\left(l - \frac{N}{2}\right)^2 + \left(p - \frac{N}{2}\right)^2\right]\right\}, \quad (2)$$

where N is the number of array elements in each dimension. The α parameter determines the initial duty cycle of the phase grating, while β determines the initial phase modulation depth of the grating. The initial choices of α and β affect the convergence of the algorithm as well as the accuracy of the resulting solution. Various combinations of initial values were tried until an acceptable solution was found. In our optimization routine the initial starting values of $\alpha = 10.0$ and $\beta = 3.0$ resulted in the solution described in Subsection 2.B. The size of the array was $N \times N$ with $N = 128$, and the continuous phase profile was quantized into $M = 16$ levels. Also, the algorithm was terminated after 100 iterations ($\sim$20 CPU min. on a VAX 3600 computer). The quality of the solution was evaluated based on two figures of merit: the total diffraction efficiency of the grating η_t and the maximum reconstruction error $\Delta R_{\max}$.

The total diffraction efficiency represents the fraction of the total input power contained within the diffraction orders of interest and is defined (in one dimension for simplicity) as

$$\eta_t = \frac{\sum_{m=N/2-K}^{N/2+K} P[m]}{\sum_{m=0}^{m=N-1} P[m]}, \quad (3)$$

where $P[(N/2) + q] \equiv \eta_q$ is the power contained in the qth diffraction order, or, equivalently, the diffraction efficiency of the qth diffraction order, and K represents the maximum diffraction order of interest. For example, $K = 5$ for a 1-to-11 fan-out grating. In general, one seeks to maximize η_t since it represents the total amount of useful power directed in the desired directions.

The reconstruction error $\Delta R[q]$ for each order q, where q is an integer in the range $[-K, K]$, is obtained (again, in one dimension for simplicity) by

$$\Delta R[q] = \frac{|\eta_q/\eta_t - \eta_q^{\text{ideal}}/\eta_t^{\text{ideal}}|}{\eta_q^{\text{ideal}}/\eta_t^{\text{ideal}}}, \quad (4)$$

where η_q is the diffraction efficiency of the qth diffraction order of the optimized grating, η_q^{ideal} is the ideal diffraction efficiency of the qth diffraction order, η_t is the total diffraction efficiency of the optimized grating, and η_t^{ideal} is the ideal total diffraction efficiency. As in Eq. (3), η_t^{ideal} is defined as

$$\eta_t^{\text{ideal}} = \frac{\sum_{m=N/2-K}^{N/2+K} P_{\text{ideal}}[m]}{\sum_{m=0}^{N-1} P_{\text{ideal}}[m]}, \quad (5)$$

where $P_{\text{ideal}}[m]$ is the ideal Gaussian power spectrum. We can then take the maximum reconstruction error

$$\Delta R_{\max} \equiv \max_q \Delta R[q] \quad (6)$$

among all the orders as our figure of merit. The reconstruction error quantifies the degree to which the grating power spectrum approximates the ideal Gaussian power spectrum.

Therefore the goal in designing free-space optical interconnects is to achieve high total diffraction efficiencies and low reconstruction errors. The results of the phase optimization are presented below.

B. Results

Figures 2(a) and 2(b) plot the ideal 2-D Gaussian power spectrum and the power spectrum of the optimized multilevel phase grating, respectively. The Fig. 3 plot slices through the peaks of the power

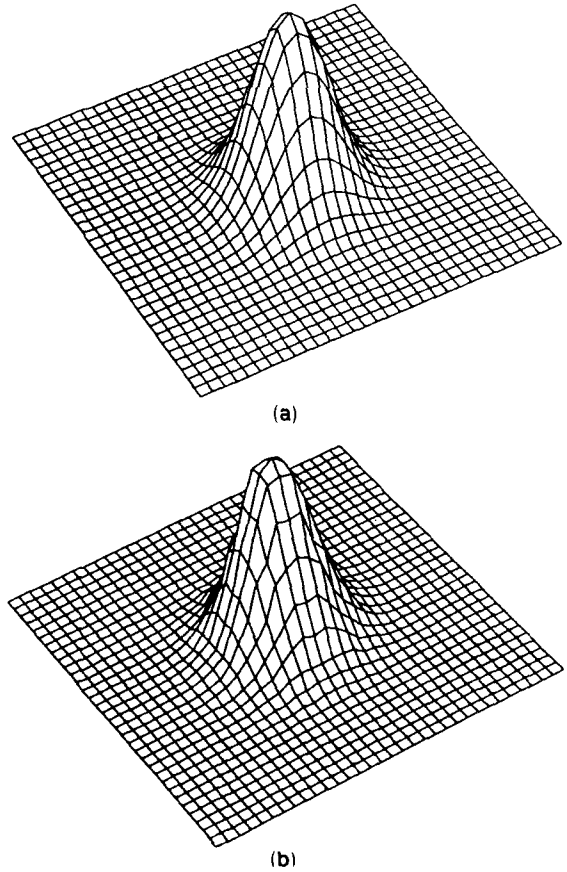

(a)

(b)

Fig. 2. 2-D power spectra: (a) ideal Gaussian, (b) optimized grating.

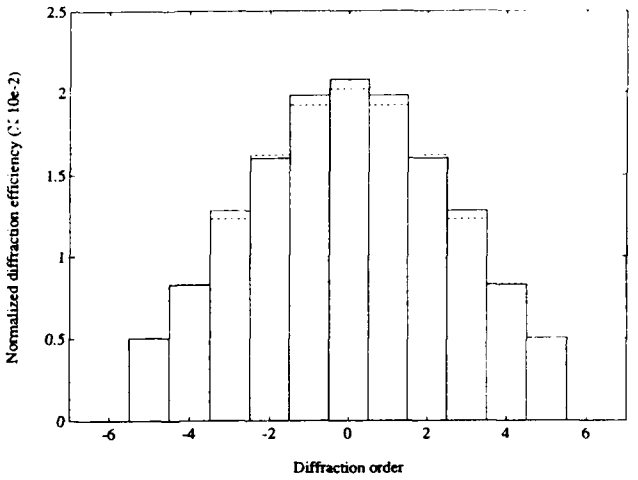

Fig. 3. Cross section of 2-D power spectra shown in Fig. 2: ideal Gaussian (dashed curve) and optimized grating (solid curve).

spectra in Fig. 2 (each normalized to the respective total diffraction efficiency). As shown, the agreement is quite good. The maximum reconstruction error among these diffraction orders is 0.0385, and the total diffraction efficiency of the optimized grating is 0.85.

These results are for a quantization into 16 equally spaced phase levels. In general, lower reconstruction errors and higher diffraction efficiencies can be obtained for finer quantization. A trade-off exists, however, if finer quantization is desired. In particular, the fabrication of the corresponding surface-relief structure becomes exceedingly difficult as the degree of quantization increases. Section 3 outlines briefly the grating fabrication process and presents the results of the fabrication of the above multilevel surface-relief structure.

3. Grating Fabrication

A. Background

Figure 4 summarizes the binary-optics fabrication process used to fabricate the Gaussian fan-out element. Optical lithography and reactive-ion etching, technologies borrowed from the semiconductor integrated circuit industry, are used in forming the surface-relief structure. To fabricate a surface-relief structure with 2^L levels, we must design L lithographic masks, and L lithography–etching steps are required, as shown. For $L > 1$ an optical alignment is performed between each lithography—etching step.

Binary surface-relief structures (i.e., $L = 1$), however, can be fabricated without optical alignment, which becomes increasingly difficult as the degree of quantization increases and the feature sizes decrease. For this reason binary gratings are relatively easier to fabricate than multilevel gratings. However, as mentioned earlier, the relative ease of fabrication comes at the expense of higher reconstruction errors and lower diffraction efficiencies. A more detailed explanation of the fabrication process for both binary and multilevel surface-relief structures can be found elsewhere.[9]

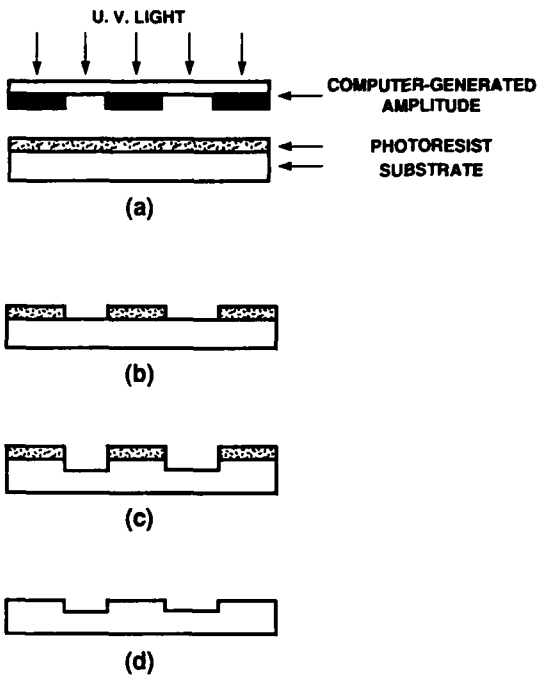

Fig. 4. Binary-optics fabrication process: (a) optical lithography, (b) development of photoresist, (c) reactive-ion etching, (d) removal of photoresist.

Two errors that are generally present in the fabrication of both binary and multilevel surface-relief gratings are etch-depth and linewidth-reproduction errors. The computer modeling of the effects of such errors on the diffraction characteristics of surface-relief gratings is a current area of research. Using a Fourier-optics formalism, one can show that for binary phase gratings the effect of an etch-depth error is to change the relative ratio of the zero-order diffraction efficiency to the higher-order diffraction efficiencies, while keeping the relative ratio of diffraction efficiencies among the higher orders (i.e., η_k/η_l, where $k \neq 0$, $l \neq 0$, and $k \neq l$) constant. For binary gratings that implement free-space optical interconnects, as the degree of fan-out increases, the sensitivity of the zero-order diffraction efficiency also increases.[12] For multilevel gratings an etch-depth error also primarily affects the zero-order diffraction efficiency; however, the relative ratio of diffraction efficiencies among the higher orders does not in general remain constant.

Note that the above statements are based on a Fourier-optics formalism of grating diffraction; consequently, they can be used reliably to analyze the diffraction behavior of actual surface-relief gratings when the period-to-wavelength ratio is large. The diffraction behavior of a representative binary surface-relief grating as a function of the period-to-wavelength ratio is considered in Section 5.

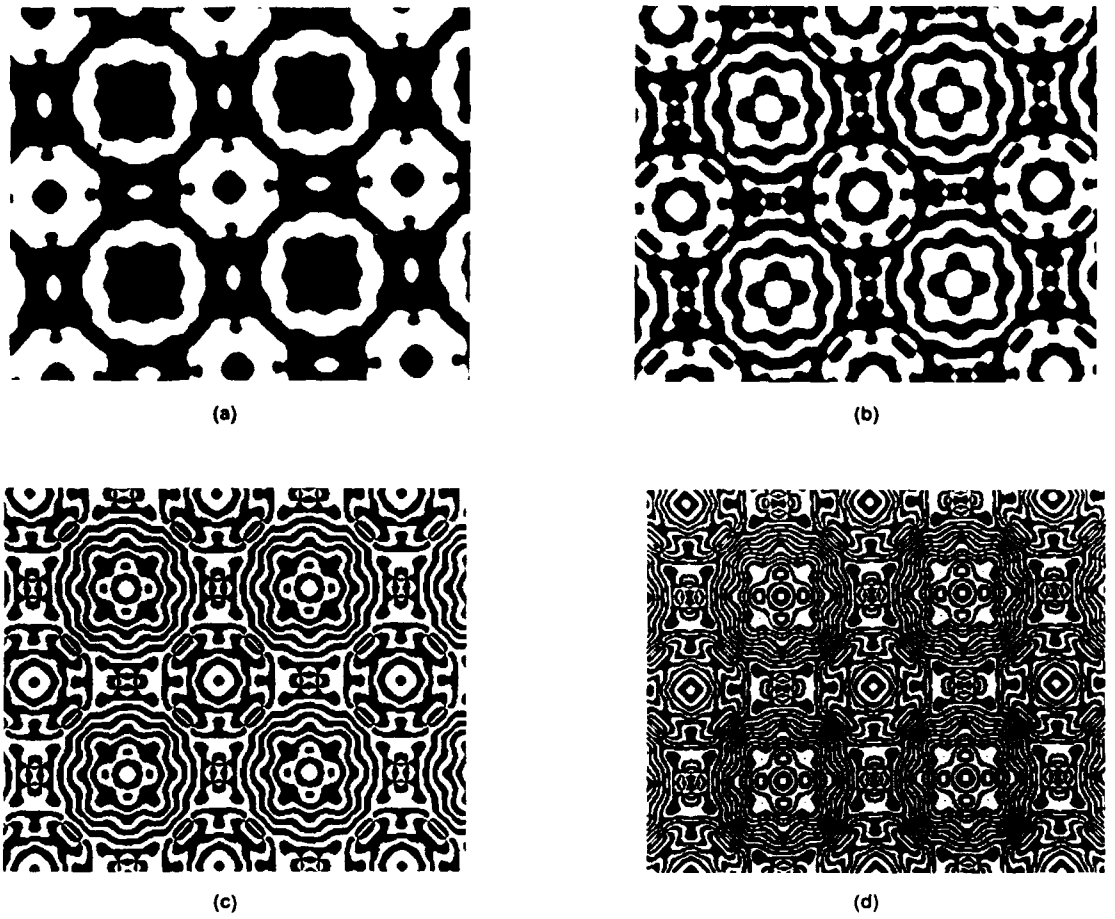

Fig. 5. Portions of lithographic masks for 16-level optimized grating: (a) mask 1, (b) mask 2, (c) mask 3, (d) mask 4.

B. Results

Four lithographic masks were designed and used to fabricate the optimized 16-level surface-relief grating described above. Portions of these masks are shown in Fig. 5. A scanning electron micrograph of the fabricated grating is shown in Fig. 6. The grating period is 128 μm. Table 1 summarizes the target etch depths and etch errors for each etching step in the fabrication process. Actual etch depths were determined from averaging measurements taken at several locations across the grating structure. As shown, the measured etch depths are within 2.6% of the target values.

Fig. 6. Scanning electron micrograph of fabricated grating.

4. Experimental Results

A He–Ne ($\lambda = 0.6328$ μm) laser was used to illuminate the grating in the experimental setup. Figure 7 plots the measured and expected power spectra of the multilevel grating (for the orders of interest). The expected power spectrum was calculated by using a Fourier-optics formalism and accounts for the etch-depth errors in the grating fabrication described

Table 1. Target Etch Depths and Etch-Depth Errors

Mask	Target Etch Depth (nm)	Etch-Depth Error (nm)
1	692.3	+17.5
2	346.2	+4.0
3	173.1	+4.4
4	86.5	+1.0

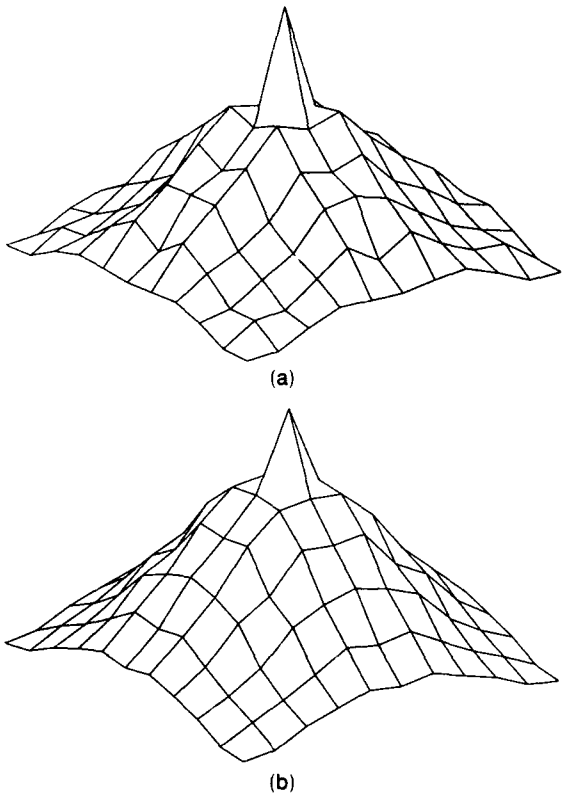

Fig. 7. 2-D power spectra of a multilevel grating: (a) measured, (b) expected.

above. Comparing the spectra in Figs. 2(b) and 7(b), we see that the primary effect of an etch-depth error is to increase the zero-order diffraction efficiency.

Figure 8 plots cross sections through the peaks of the 2-D power spectra (each normalized to the total diffraction efficiency) shown in Fig. 7. With the exception of the zero order, the two spectra are in agreement. Table 2 summarizes the reconstruction errors for the orders shown in Fig. 8.

The relatively large reconstruction error for the zero order is consistent with the observation that the

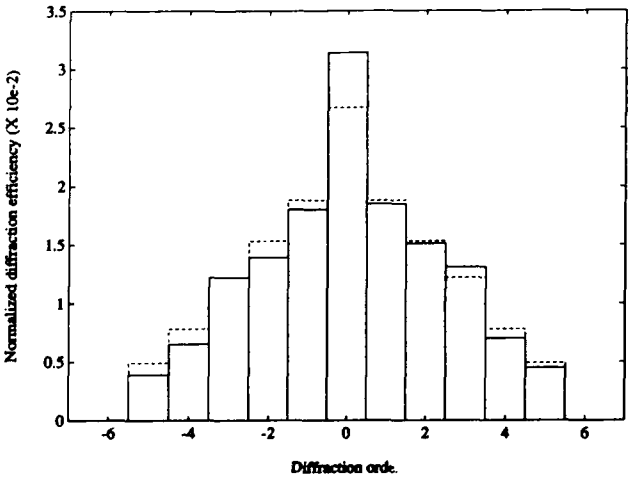

Fig. 8. Cross section of 2-D power spectra shown in Fig. 7: measured (solid curve), expected (dashed curve).

Table 2. Reconstruction Errors for Measured Power Spectrum

q	$\Delta R\|q\|$
−5	0.208
−4	0.177
−3	0.00230
−2	0.0897
−1	0.0427
0	0.178
1	0.0150
2	0.0125
3	0.0794
4	0.110
5	0.0724

actual zero-order diffraction efficiency of surface-relief gratings is generally higher than the corresponding zero-order diffraction efficiency predicted by using a Fourier-optics formalism.[12,13] Recall that Fourier theory (i.e., scalar diffraction theory) provides reliable estimates of grating diffraction behavior for large (i.e., approaching infinity) period-to-wavelength ratios. Rigorous analyses of surface-relief gratings have been performed that investigate the deviations of the diffraction behavior from that predicted by a Fourier-optics analysis.[12,13] Section 5 presents the results of such an analysis for a representative binary surface-relief grating.

The reconstruction errors for the negative-fifth and negative-fourth orders are also relatively high. The absolute deviation in power, however, is quite small. For certain applications such as optical switching, in which a certain threshold power must be reached, it is the absolute, as opposed to the fractional, deviation in power that is the more critical; however, other applications such as neural computing, in which the relative power contained in each order is tailored to implement a set of interconnection strengths, require small fractional deviations (i.e., low reconstruction errors). Therefore the information conveyed by the concept of the reconstruction error must be interpreted with an application in mind.

Another feature of Fig. 8 is that the measured spectrum has a slight asymmetry. In theory the power spectrum must be symmetric since the surface-relief structure itself is symmetric (e.g., see lithographic masks in Fig. 5). Therefore we can conclude that the surface-relief structure is not symmetric.

The occurrence of fabrication errors such as nonuniform etch depths, misalignment, and nonvertical sidewalls are all plausible explanations for the observed asymmetry in the measured power spectrum. The lack of computer models for analyzing the effects of such fabrication errors on the power spectra of diffraction gratings along with the fact that it is extremely difficult to experimentally measure and determine the nonuniformities in a surface-relief profile owing to such fabrication errors precludes a detailed analysis of the experimentally measured power spectrum.

An important point to note is that the minimum feature size on the surface-relief structure shown in Fig. 6 is of the order of the wavelength of light. Recall that scalar diffraction theory breaks down when the dimensions of the diffracting features of the grating approach the wavelength of light. Therefore the Fourier-optics formalism used to determine the expected power spectrum in Fig. 2(b) may not model reliably the diffraction characteristics of the fabricated grating. This fact, however, does not explain the observed asymmetry since a rigorous analysis of the fabricated grating would also yield a symmetric power spectrum, owing to the symmetry of the surface-relief profile.

As shown above, deviations exist between the measured and predicted power spectra (see Figs. 2 and 8). These deviations can be explained, in part, by the fact that the predicted spectrum was calculated by using a scalar diffraction theory. A scalar theory, unlike a rigorous electromagnetic wave theory, does not account for the polarization of the incident light. When the grating period Λ is large compared with the wavelength of the incident light λ, the grating diffraction behavior is independent of the incident polarization. In such a situation, scalar diffraction theory can be used to obtain reliable estimates of the grating diffraction behavior. However, when the dimensions of the diffracting features of the grating approach the wavelength of the incident light, polarization effects dominate and therefore must be taken into account.

For our multilevel surface-relief grating (see Fig. 6) the minimum feature size is 1 μm. Therefore scalar diffraction theory cannot be expected to give reliable estimates of the diffraction behavior of our grating. For this reason we proceeded to investigate the behavior of surface-relief gratings as a function of the period-to-wavelength ratio Λ/λ. Presently, computer models that can analyze the diffraction behavior of arbitrary 2-D surface-relief gratings do not exist. However, models exist that can analyze arbitrary 1-D grating structures. For simplicity we chose to analyze a representative binary surface-relief grating. The results of this analysis are presented in Section 5.

5. Scalar-Theory Design Limitations

Optimized phase profiles for free-space optical interconnects are, in practice, implemented with surface-relief structures. Such an implementation is a good one when the physical period of the surface-relief grating is large compared with the wavelength of the incident light. In this section we analyze the diffraction behavior of a binary surface-relief grating as a function of the period-to-wavelength ratio. This surface-relief grating is a practical implementation of an optimized binary phase grating[14] that achieves a 1-to-5 uniform fan-out. A rigorous vector coupled-wave theory of grating diffraction, developed by Moharam and Gaylord,[8] is employed. A computer code based on this theory is used to perform the analysis. In our simulations the incident medium is air and the grating medium is fused silica (index of refraction $n = 1.5$). Also, the maximum period-to-wavelength ratio considered was 50 for practical reasons (i.e., necessary computation times).

We note that our analysis is specific to the particular grating considered. A similar analysis for arbitrary grating structures will in general give different results. It is not our intention to make general statements on grating behavior as a function of the period-to-wavelength ratio. In fact, it is not clear whether such a generalization can be made. The main purpose of our analysis is to illustrate qualitatively the effect of the period-to-wavelength ratio on the performance of surface-relief gratings that implement free-space optical interconnects.

The breakdown of scalar diffraction theory manifests itself in grating diffraction with the onset of polarization effects. As the period-to-wavelength ratio decreases, the grating power spectrum becomes sensitive to the polarization of the incident light. In the limit of a large period-to-wavelength ratio the grating power spectrum becomes independent of the polarization of the incident light; consequently, light can be treated as a scalar quantity, as opposed to a vector quantity.

Figures 9(a), 9(b), and 9(c) plot the grating power spectra for period-to-wavelength ratios of 2, 15, and 50, respectively (dashed curves), and the power spectrum predicted using a Fourier-optics formalism of grating diffraction (solid curves). In these plots, only the orders from -2 to $+2$ are shown and the incident polarization is TE. The key feature of these plots is that the diffraction behavior deviates significantly from that predicted by the Fourier theory when the period-to-wavelength ratio is small. Conversely, when the period-to-wavelength ratio is large, the diffraction behavior of actual surface-relief gratings can be modeled accurately with a Fourier-optics formalism.

Figure 10 plots the maximum reconstruction error versus the period-to-wavelength ratio for both TE and TM incident polarizations. The minimum period-to-wavelength ratio considered was 2. This value was chosen such that at least five orders were propagating in both the incident medium and the grating medium. There are three important features of this plot.

First, as the period-to-wavelength ratio increases, the TE and TM curves approach each other. This result is reasonable since we know that in the limit of an infinite period-to-wavelength ratio the two cases are degenerate.

Second, at small and moderate values of the period-to-wavelength ratio the maximum reconstruction errors for the TE- and TM-polarized incident waves deviate significantly. The particularly low value of the maximum reconstruction error for the TM-polarized case at a period-to-wavelength ratio of 9 is an unexpected result. The maximum reconstruction error at this point is 0.0287, which is even lower

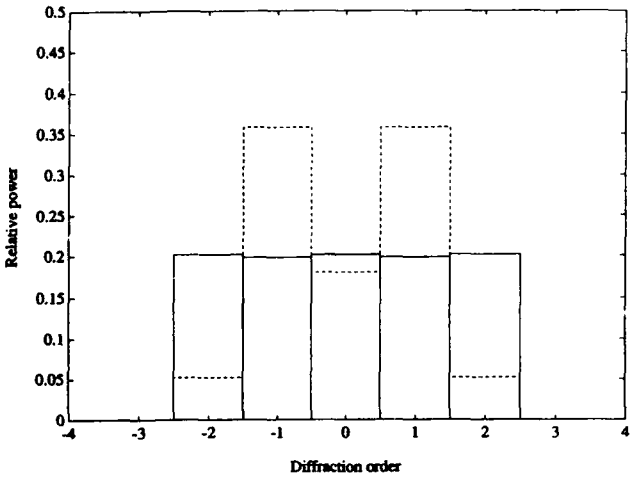

(a)

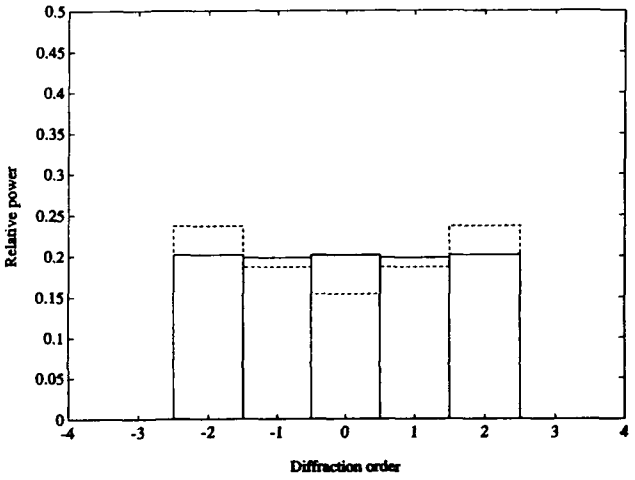

(b)

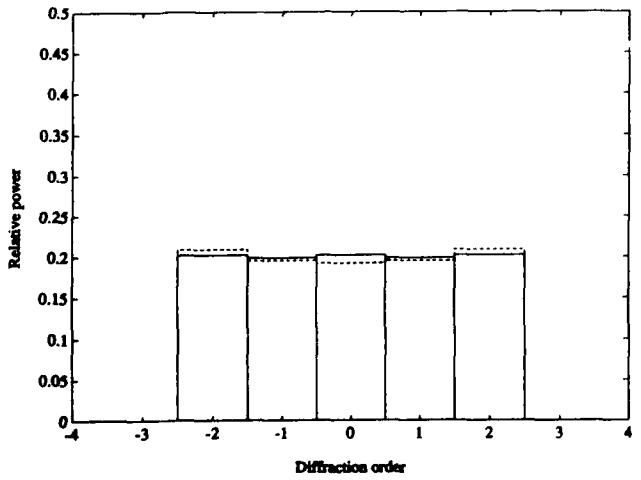

(c)

Fig. 9. Power spectrum of a 1-to-5 fan-out grating for various period-to-wavelength ratios Λ/λ with TE incident polarization: (a) 2.0, (b) 15.0, (c) 50.0. Rigorous calculation is denoted by the dashed curve; the Fourier-optics prediction is denoted by the solid curve.

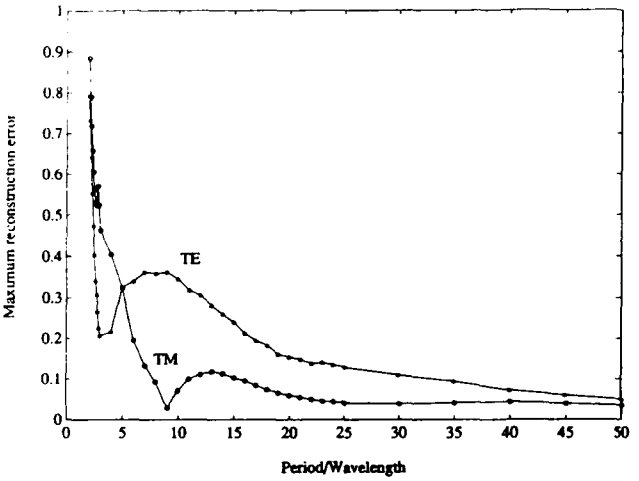

Fig. 10. Maximum reconstruction error versus period-to-wavelength ratio for a 1-to-5 fan-out grating and TE and TM incident polarizations.

than the maximum reconstruction error at a period-to-wavelength ratio of 50, 0.0348. The grating power spectrum for an incident TM-polarized wave and a period-to-wavelength ratio of 9 is shown in Fig. 11 along with the ideal power spectrum predicted from a Fourier-optics formalism. Although this anomaly cannot be generalized to describe the diffraction characteristics of arbitrary grating structures, further investigation and research on grating diffraction as a function of the period-to-wavelength ratio may enable designers to utilize occurrences such as this in small, compact optical systems.

The last point to note is that Fig. 10 contains no information on the actual amount of power contained in each of the transmitted diffraction orders. For example, the plot shows that, at a period-to-wavelength ratio of 5, both the TE- and TM-polarized cases have a maximum reconstruction error of approximately 0.32; however, Fig. 12 shows that the power

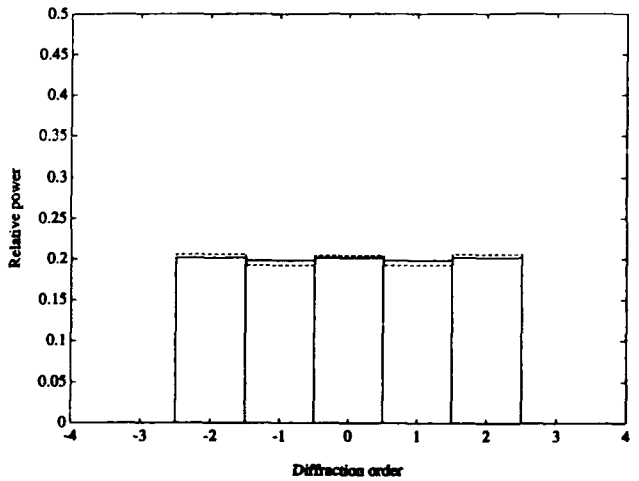

Fig. 11. Power spectrum of a 1-to-5 uniform fan-out grating for $\Lambda/\lambda = 9$ and TM incident polarization. Rigorous calculation is denoted by the dashed curve; the Fourier-optics prediction is denoted by the solid curve.

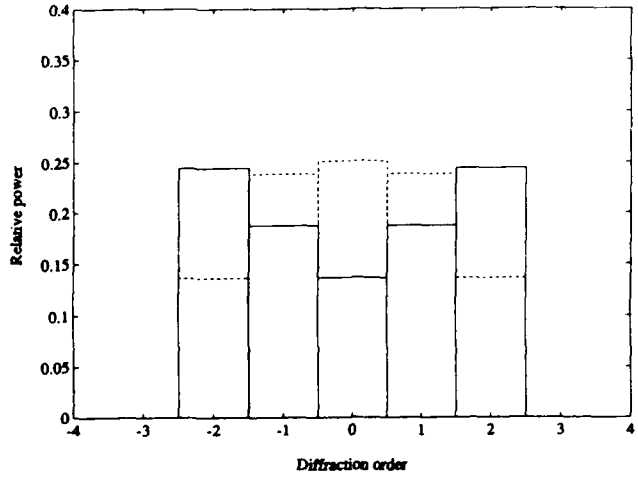

Fig. 12. Power spectrum of a 1-to-5 uniform fan-out grating for $\Lambda/\lambda = 5$ and TE (solid curve) and TM (dashed curve) incident polarizations.

spectra for these two polarizations differ dramatically.

Figure 13 plots the total diffraction of the 1-to-5 uniform fan-out grating as a function of the period-to-wavelength ratio for both TE- and TM-polarized incident waves. As expected, the diffraction efficiency is independent of polarization for large values of the period-to-wavelength ratios, and polarization effects become apparent as the period-to-wavelength ratio decreases. These effects, however, are not as dramatic as those for the reconstruction error.

Figure 13 also shows that high total diffraction efficiencies are possible for small period-to-wavelength ratios. Physically, the increase in total diffraction efficiency for small period-to-wavelength ratios is caused by the number of propagating (i.e., nonzero time-averaged power) diffraction orders in the grating medium decreasing as the period-to-wavelength ratio decreases. In theory it is possible to achieve a total diffraction efficiency of 100% (ignoring Fresnel losses) by decreasing the period-to-wavelength ratio. However, one must remember that the reconstruction error increases a great deal as the period-to-wavelength ratio decreases. Therefore a trade-off exists between achieving a high total diffraction efficiency and a low maximum reconstruction error. The optimum value of the period-to-wavelength ratio is determined by the particular application at hand (e.g., optical switching–thresholding, beam combining, or optical implementation of the synaptic interconnections of a neural network).

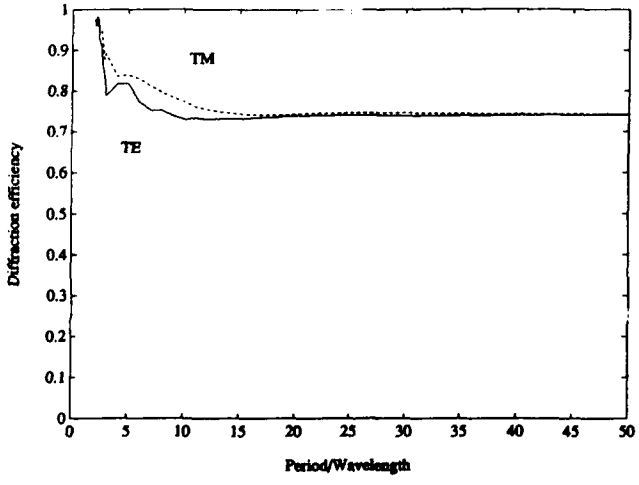

Fig. 13. Total diffraction efficiency versus period-to-wavelength ratio for a 1-to-5 uniform fan-out grating with TE (solid curve) and TM (dashed curve) incident polarizations.

6. Summary

A modified Gerchberg–Saxton phase-retrieval algorithm has been used to optimize phase profiles that can be fabricated by using binary-optics fabrication technology. An optimized multilevel phase grating that achieves a 2-D Gaussian fan-out was described. The total theoretical diffraction efficiency of the grating is 85%, and the theoretical maximum reconstruction error is 3.8%. A surface-relief structure that implemented the optimized phase grating was fabricated. Good etch-depth control was achieved (<3% error); however, the measured grating power spectrum lacked symmetry. This fact was attributed to various fabrication errors such as nonuniform etch depths, nonvertical sidewalls, and misalignment of the various mask levels.

Finally, theoretical limitations on the implementation of optimized phase profiles (i.e., determined from phase optimization techniques such as phase retrieval or simulated annealing) with surface-relief structures were discussed. In particular, the use of scalar diffraction theory, valid for large period-to-wavelength ratios, to describe grating diffraction was addressed. The performance of a binary surface-relief grating was analyzed as a function of the period-to-wavelength ratio. The performance was evaluated based on the maximum reconstruction error and the total diffraction efficiency.

The authors thank several colleagues: Alan Waxman for the development of the application, Margaret Stern and Marsden Griswold for fabricating the multilevel surface-relief grating and for taking the scanning electron micrograph of this grating, and Robert Knowlden and Edward Motamedi for help in the mask design. This work was funded by the Defense Advanced Research Projects Agency.

References

1. H. Dammann and E. Klotz, "Coherent optical generation and inspection of two-dimensional periodic structures," Opt. Acta **24**, 505–515 (1977).
2. J. N. Mait, "Review of multi-phase Fourier gating design for array generation," in *Computer and Optically Formed Holographic Optics*, I. Cindrich and S. H. Lee, eds., Proc. Soc. Photo-Opt. Instrum. Eng. **1211**, 67–78 (1990).
3. K. Heggarty, R. Chevallier, Y. Idan, and G. Y. Sirat, "An opto-electronic implementation of a neural network," in *Opti-*

cal Interconnections and Networks, H. Bartelt, ed., Proc. Soc. Photo-Opt. Instrum. Eng. **1281,** 136–144 (1990).
4. N. H. Farhat, "Optoelectronic analogs of self-programming neural nets: architecture and methodologies for implementing fast stochastic learning by simulated annealing," Appl. Opt. **26,** 5093–5103 (1987).
5. S. Kirkpatrick, C. D. Gelatt, and M. P. Vecchi, "Optimization by simulated annealing," Science **220**, 671–680 (1983).
6. R. W. Gerchberg and W. O. Saxton, "A practical algorithm for the determination of phase from image and diffraction plane pictures," Optik **35,** 237–246 (1972).
7. D. A. Fay and A. M. Waxman, "Neurodynamics of real-time image velocity extraction," in *Neural Networks for Vision and Image Processing*, G. Carpenter and S. Grossberg, eds. (MIT Press, Cambridge, Mass., 1992), pp. 221–246.
8. M. G. Moharam and T. K. Gaylord, "Diffraction analysis of dielectric surface-relief gratings," J. Opt. Soc. Am. **72,** 1385–1392 (1982).
9. G. J. Swanson, "Binary optics technology: the theory and design of multi-level diffractive optical elements," Tech. Rep. 854 (MIT Lincoln Laboratory, Cambridge, Mass., 1989).
10. J. R. Fienup, "Iterative method applied to image reconstruction and to computer-generated holograms," Opt. Eng. **19,** 297–305 (1980).
11. J. R. Fienup and C. C. Wackerman, "Phase-retrieval stagnation problems and solutions," J. Opt. Soc. Am. A **3,** 1897–1907 (1986).
12. V. V. Wong, "Theoretical and practical limits on the design and fabrication of free-space optical interconnects," M.S. thesis (Massachusetts Institute of Technology, Cambridge, Mass., 1991).
13. A. Vasara, E. Noponen, J. Turunen, J. M. Miller, and M. R. Taghizadeh, "Rigorous diffraction analysis of Dammann gratings," Opt. Commun. **81,** 337–342 (1991).
14. J. R. Leger, G. J. Swanson, and W. B. Veldkamp, "Coherent laser addition using binary phase gratings," Appl. Opt. **26,** 4391–4399 (1987).